



# On the finite element method for solving the oblique derivative boundary value problems and its application in local gravity field modelling

Zuzana Minarechová<sup>1</sup> · Marek Macák<sup>1</sup> · Róbert Čunderlík<sup>1</sup> · Karol Mikula<sup>1,2</sup>

Received: 31 July 2020 / Accepted: 27 May 2021  
© Springer-Verlag GmbH Germany, part of Springer Nature 2021

## Abstract

The paper presents local gravity field modelling in spatial domain using the finite element method (FEM). FEM as a numerical method is applied for solving the geodetic boundary value problem with oblique derivative boundary conditions (BC). For such a problem, we derive a new numerical scheme where the oblique derivative BC are considered directly at computational nodes on the discretized Earth's topography. Then, the developed FEM approach is tested in several artificial testing experiments as well as by a reconstruction of a known harmonic function above the extremely complicated Earth's topography in the Himalayas. A main numerical experiment is focused on very detailed local gravity field modelling in Slovakia using terrestrial gravity data. The high horizontal resolution  $100 \times 100$  m and non-uniform resolution in the radial direction has resulted in a 3D unstructured mesh of finite elements with 5,287,500,000 unknowns. Large-scale parallel computations were performed on a parallel cluster using 1.5 TB of distributed memory. The obtained local quasigeoid model is tested at 403 GNSS-levelling benchmarks. The standard deviation of residuals 2.77 cm, which decreases to 2.54 cm after excluding 7 outliers, indicates its high precision. However, depicted residuals show their low-frequency character with amplitudes about  $\pm 3$  cm. As a by-product, the first and second derivatives of the obtained disturbing potential in the radial direction are also evaluated in several altitude levels as well as on the Earth's surface. Finally, the paper presents a comparison of the obtained FEM solution with the recent local quasigeoid models in Slovakia computed in the spatial as well as spectral domain. It illustrates a practical contribution of the presented FEM approach for precise local gravity field modelling, especially in high mountains.

**Keywords** Finite element method · Local gravity field modelling · Oblique derivative boundary value problem

## 1 Introduction

The determination of the Earth's gravity field is usually formulated in terms of the geodetic boundary value problems (BVPs). Nowadays, precise 3D positioning of terrestrial gravimetric measurements by GNSS directly provides sur-

face gravity disturbances that represent the oblique derivative boundary conditions (BC) of the fixed gravimetric boundary value problem (FGBVP). Hence, from the mathematical point of view, the FGBVP represents an exterior oblique derivative geodetic BVP for the Laplace equation, cf. Koch and Pope (1972), Freeden and Kersten (1981), Bjerhammar and Svensson (1983) and Holota (1997).

A standard procedure to solve the oblique derivative BVP has been based on integral equations using the single-layer potential, cf. Bitzadse (1968) and Miranda (1970). Later Koch and Pope (1972) applied such an integral equation procedure to solve the FGBVP. However, the strong nature of the singularities demanding Cauchy's principal integral values turned out to be a serious obstacle, see Freeden and Gerhards (2013). Later, Freeden and Kersten (1981) proposed a new concept of approximations using the generalized Fourier expansions to transfer strongly singular integrals into regular ones. This approach has been further developed in Freeden

✉ Zuzana Minarechová  
minarechova@math.sk

Marek Macák  
macak@math.sk

Róbert Čunderlík  
cunderli@svf.stuba.sk

Karol Mikula  
mikula@math.sk

<sup>1</sup> Faculty of Civil Engineering, Slovak University of Technology, Radlinského 11, 810 05 Bratislava, Slovakia

<sup>2</sup> Algoritmy:SK s.r.o., Šulekova 6, 81106 Bratislava, Slovakia

(1987), Bauer (2004), Gutting (2007, 2012), Freeden and Michel (2004) and Freeden and Gerhards (2013). Recently, Freeden and Nutz (2017) published the conceptual setup of the Runge–Walsh theorem for the oblique derivative problem of physical geodesy.

An expansion of high-performance computing (HPC) facilities has brought new ways and opportunities in solving various engineering problems, including the Earth's gravity field modelling. Efficient numerical methods such as the boundary element method (BEM), the finite element method (FEM), the finite difference method (FDM) or the finite volume method (FVM) have been applied for gravity field modelling. Main advantages of these numerical approaches in gravity field modelling are a straightforward refinement of the discretization, opportunity to consider real topography as well as feasibility for high-resolution modelling.

The first innovative studies on numerical methods applied to gravity field modelling were introduced in the 1980s, and they were based on FEM, cf. Meissl (1981) or Shaofeng and Dingbo (1991). In the 1990s, the FDM was studied by Keller (1995) and the indirect BEM approach was developed by Klees (1995) and Lehmann and Klees (1999). This approach was later improved by numerical techniques that have significantly reduced numerical complexity of the problem; see Klees et al. (2001). Later on, the direct BEM approach was introduced by Čunderlík et al. (2008) or Čunderlík and Mikula (2010). The oblique derivative problem treated by BEM was discussed in Čunderlík et al. (2012). At that time, new studies on FEM were developed and published by Fašková et al. (2007) or Fašková et al. (2010), Šprlák et al. (2011) and recently by Mráz et al. (2016). However, none of these approaches has considered the oblique derivative BC in their concepts. On the other hand, FEM for the elliptic partial differential equations with the oblique derivative BC on 2D curved domains has been studied by Barrett and Elliott (1985) and recently by Kawecki (2019) and Gallistl (2019).

The first application of FVM to gravity field modelling was introduced by Fašková (2008) and its parallel implementation by Minarechová et al. (2015). However, both papers have studied the geodetic BVP with the Neumann BC. The first insight of FVM applied to the oblique derivative BVP has been discussed in Macák et al. (2012). Later this effort was further developed in Macák et al. (2014) and Macák et al. (2015), where a treatment of the oblique derivative by the central scheme and the first-order upwind scheme, respectively, was introduced for solving FGBVPs on uniform grids. Recently, Medl' a et al. (2018) have presented the FVM for solving the oblique derivative BVP on 3D unstructured meshes above the real Earth's topography. As an improvement, the authors of Droniou et al. (2019) have developed an approach where the oblique derivative BC is treated in the way that its tangential component is considered as an advective

tion along the Earth's topography regularized by a carefully designed surface diffusion term.

In this paper, we continue in our studies on FEM published by Fašková et al. (2010) and recently by Macák et al. (2020). The main difference with the latter one is in applying the oblique derivative BC. In the previous FEM approach, it is considered as an average value on the bottom side of finite elements using two tangential vectors and the same values of the oblique derivative for all nodes on the bottom side of the element. This led to instabilities for larger oblique angles reported in Macák et al. (2020). In this work, the oblique derivative is incorporated directly into the computational nodes using two tangential vectors for each node. Such an approach should reduce a loss of accuracy. The developed method is tested in 3 artificial testing experiments (Sect. 4.1) and by a reconstruction of the harmonic function (EGM2008) above the extremely complicated Earth's topography in the Himalayas and Tibetan Plateau (Sect. 4.2). In Sect. 4.3, we focus on high-resolution local gravity field modelling in Slovakia using terrestrial gravity data. Our aim and challenge is to reach similar or better accuracy as the recent local quasi-geoid models obtained by (i) completely different approach based on a combination of spherical harmonics, band-limited spherical radial basis functions and the residual terrain model technique (Bucha et al. 2016), and by (ii) applying the aforementioned FVM approach (Droniou et al. 2019) with the results presented in Čunderlík et al. (2020).

## 2 Formulation of the oblique derivative BVP

Let us consider the FGBVP, cf. (Koch and Pope 1972; Bjerhammar and Svensson 1983; Holota 1997):

$$\Delta T(\mathbf{x}) = 0, \quad \mathbf{x} \in R^3 - S, \quad (1)$$

$$\nabla T(\mathbf{x}) \cdot \mathbf{s}(\mathbf{x}) = -\delta g(\mathbf{x}), \quad \mathbf{x} \in \partial S, \quad (2)$$

$$T(\mathbf{x}) \rightarrow 0, \quad \text{as } |\mathbf{x}| \rightarrow \infty, \quad (3)$$

where  $S$  is the Earth or more generally any Lipschitz domain,  $T(\mathbf{x})$  is the disturbing potential defined as a difference between the real and normal gravity potential at any point  $\mathbf{x} = (x, y, z)$ ,  $\delta g(\mathbf{x})$  is the gravity disturbance, and the vector  $\mathbf{s}(\mathbf{x}) = -\nabla U(\mathbf{x})/|\nabla U(\mathbf{x})|$  is the unit vector normal to the equipotential surface of the normal potential  $U(\mathbf{x})$  at any point  $\mathbf{x}$ . Eqs. (1)–(3) represent an exterior BVP for the Laplace equation, where the computational domain lies outside the Earth and is infinite.

However, FEM requires a discretization of the whole computational domain into finite elements. To that goal we construct a bounded domain  $\Omega$  in the external space above the Earth, see Fašková et al. (2010). Such a domain  $\Omega$  (Fig. 1) is bounded by the bottom surface  $\Gamma \subset \partial\Omega$  representing a

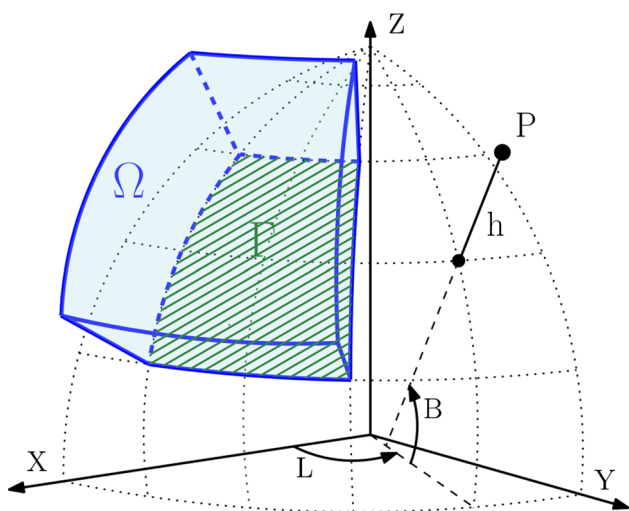


**Fig. 1** The computational domain  $\Omega$ . The domain  $\Omega$  is delimited by blue edges; the bottom surface  $\Gamma \subset \partial\Omega$  hatched by green colour represents a chosen part of the Earth’s surface;  $B, L, h$  coordinates denote ellipsoidal latitude, longitude and height, respectively

part of the Earth’s surface and an upper surface created at appropriate altitude, e.g. at a mean altitude of the GOCE satellite orbits. In case of local gravity field modelling, the domain  $\Omega$  is also bounded by four side boundaries (Fig. 1). Then, on the top and side boundaries, the Dirichlet-type BC for the disturbing potential can be prescribed.

In the bounded domain  $\Omega$ , we consider the following BVP

$$\Delta T(\mathbf{x}) = 0, \quad \mathbf{x} \in \Omega \subset \mathbf{R}^3, \tag{4}$$

$$\nabla T(\mathbf{x}) \cdot \mathbf{s}(\mathbf{x}) = -\delta g(\mathbf{x}), \quad \mathbf{x} \in \Gamma \subset \partial\Omega, \tag{5}$$

$$T(\mathbf{x}) = T_{SAT}(\mathbf{x}), \quad \mathbf{x} \in \partial\Omega - \Gamma, \tag{6}$$

where  $\Gamma \subset \partial\Omega$  represents the part of the Earth’s topography,  $\partial\Omega - \Gamma$  represents the top boundary together with side boundaries, and  $T_{SAT}$  is the disturbing potential generated from any GRACE/GOCE-based satellite-only geopotential model.

It is worth noting that by considering the artificial condition (6) we abandon the condition of regularity at infinity (3). Instead at infinity, the solution is fixed to the GRACE/GOCE-based geopotential models on the upper boundary which is chosen approximately at altitude of the GOCE satellite orbits. In this way, we utilize information about the gravity field detected by the satellite missions, however, at altitudes of their observations. Moreover, in the case of local gravity field modelling ‘purely’ in the spatial domain, this artificial condition (6) allows us to overcome a problem of integrating over the whole globe. Such a treatment conceptually differs from classical approaches based on the well-known ‘remove-compute-restore’ strategy.

### 3 The FEM solution to the oblique derivative BVP

In our approach, we follow the fundamental principles of FEM published in Reddy (2006).

#### 3.1 The finite element discretization

The FEM is a numerical method that assumes discretization of the whole computational domain  $\Omega$  by a union of elements  $\Omega^e, e = 1, \dots, N$ , where  $N$  denotes the number of elements in the domain  $\Omega$ . For our problem, we will use the hexahedral elements with eight nodes, see Brenner and Scott (2002) or Reddy (2006), and we will divide the computational domain into  $n_1, n_2, n_3$  elements in latitudinal, longitudinal and altitudinal direction, respectively. Then, the number of elements in the domain  $\Omega$  will be  $N = n_1 n_2 n_3$ . To specify the position of an element  $\Omega^e$ , we will use indexes  $k, l, m$ , where  $k = 1, \dots, n_1, l = 1, \dots, n_2$  and  $m = 1, \dots, n_3$ . It is well-known that discretization of spherical domains by polygonal elements results in the so-called discretization error. This error can be partially eliminated by using a finer discretization, so subsequent refining the computational mesh yields a convergence of the finite element domain to the original one.

#### 3.2 The weak formulation on the element

Let us consider an arbitrary element  $\Omega^e$  from our finite element discretization with indexes  $k = 1, \dots, n_1, l = 1, \dots, n_2$  and  $m = 2, \dots, n_3$ . We multiply the differential equation (4) by a weight function  $w$  and using Green’s identity (we omit  $(\mathbf{x})$  to simplify the notation in the following equations) we obtain the weak formulation of (4) over an arbitrary above defined element  $\Omega^e$

$$\int_{\Omega^e} \nabla T \cdot \nabla w \, dx dy dz = \int_{\partial\Omega^e} \nabla T \cdot \mathbf{n} w \, d\sigma, \tag{7}$$

where  $\mathbf{n}$  denotes the unit normal to  $\partial\Omega^e$ .

Since on the bottom boundary  $\Gamma$  the oblique derivative BC (5) is prescribed, for the row of elements that lie on this boundary, i. e.  $k = 1, \dots, n_1, l = 1, \dots, n_2$  and  $m = 1$ , we will use and modify (7) in the following way. We split the oblique vector  $\mathbf{s}$  into one normal and two tangential components

$$\mathbf{s} = c_1 \mathbf{n} + c_2 \mathbf{t}_1 + c_3 \mathbf{t}_2, \tag{8}$$

where  $\mathbf{n}$  is the normal vector and  $\mathbf{t}_1, \mathbf{t}_2$  are tangent vectors to  $\Gamma^e \subset \partial\Omega^e \subset \mathbf{R}^3$ , where  $\Gamma^e$  denotes the bottom boundary of an element  $\Omega^e$ . These three vectors together form an orthonormal basis.

Then, we replace vector  $\mathbf{s}$  in (5) by (8) to obtain

$$\nabla T \cdot \mathbf{s} = c_1 \nabla T \cdot \mathbf{n} + c_2 \nabla T \cdot \mathbf{t}_1 + c_3 \nabla T \cdot \mathbf{t}_2 = -\delta g. \tag{9}$$

From (9), we express the normal derivative

$$\nabla T \cdot \mathbf{n} = \frac{-\delta g}{c_1} - \frac{c_2}{c_1} \frac{\partial T}{\partial \mathbf{t}_1} - \frac{c_3}{c_1} \frac{\partial T}{\partial \mathbf{t}_2}, \tag{10}$$

where we assume that  $c_1 \neq 0$ . Remark: from the theoretical point of view,  $c_1 = 0$  if  $\mathbf{s}$  is perpendicular to  $\mathbf{n}$ . However, in practical experiments we always use a 'nonzero' horizontal resolution of the grid points that discretized the real Earth's surface. In such cases,  $\mathbf{s}$  is never perpendicular to  $\mathbf{n}$ , and thus, the assumption  $c_1 \neq 0$  is always fulfilled.

Now, we insert (10) to (7) to get

$$\begin{aligned} \int_{\Omega^e} \nabla T \cdot \nabla w \, dx dy dz &= \\ &= \int_{\Gamma^e} \left( \frac{-\delta g}{c_1} - \frac{c_2}{c_1} \frac{\partial T}{\partial \mathbf{t}_1} - \frac{c_3}{c_1} \frac{\partial T}{\partial \mathbf{t}_2} \right) w \, d\sigma \\ &+ \int_{\partial \Omega^e \setminus \Gamma^e} \nabla T \cdot \mathbf{n} \, w \, d\sigma. \end{aligned} \tag{11}$$

After some rearrangement, we have

$$\begin{aligned} \int_{\Omega^e} \nabla T \cdot \nabla w \, dx dy dz &+ \frac{c_2}{c_1} \int_{\Gamma^e} \frac{\partial T}{\partial \mathbf{t}_1} w \, d\sigma \\ &+ \frac{c_3}{c_1} \int_{\Gamma^e} \frac{\partial T}{\partial \mathbf{t}_2} w \, d\sigma \\ &= \int_{\Gamma^e} \frac{-\delta g}{c_1} w \, d\sigma + \int_{\partial \Omega^e \setminus \Gamma^e} \nabla T \cdot \mathbf{n} \, w \, d\sigma. \end{aligned} \tag{12}$$

In this way, we have obtained the weak formulation (7) or (12) of the BVP (4)–(6) on every element  $\Omega^e$  of our finite element discretization. The study of weak solution of the oblique derivative BVP is included in the book by Lieberman (2013).

### 3.3 The finite element model

For a hexahedral element  $\Omega^e$  with eight nodes, we can write

$$T \approx T^e = \sum_{j=1}^8 T_j^e \psi_j, \tag{13}$$

i. e. we take an approximation of the unknown value  $T$  as  $T^e$ , a linear combination of basis functions  $\psi_j$  with coefficients  $T_j^e$ ,  $j = 1, \dots, 8$ . We substitute it into the weak formulation

(7), namely for elements  $\Omega^e$  where indexes  $k = 1, \dots, n_1$ ,  $l = 1, \dots, n_2$  and  $m = 2, \dots, n_3$ , and consider  $\psi_i$  for weight function  $w$ . We obtain the  $i^{th}$  equation in the form

$$\begin{aligned} \sum_{j=1}^8 T_j^e \int_{\Omega^e} \frac{\partial \psi_j}{\partial x} \frac{\partial \psi_i}{\partial x} + \frac{\partial \psi_j}{\partial y} \frac{\partial \psi_i}{\partial y} + \frac{\partial \psi_j}{\partial z} \frac{\partial \psi_i}{\partial z} \, dx dy dz \\ = \sum_{j=1}^8 \int_{\partial \Omega^e} q_n \psi_i \, dx dy, \end{aligned} \tag{14}$$

where  $q_n = \nabla T \cdot \mathbf{n}$  denotes the projection of the vector  $\nabla T$  along the unit normal  $\mathbf{n}$ .

For the row of elements  $\Omega^e$  given by indexes  $k = 1, \dots, n_1, l = 1, \dots, n_2$  and  $m = 1$ , we follow the same way and after inserting (13) into (12) and considering  $w = \psi_i$ , we obtain the  $i^{th}$  equation in the form

$$\begin{aligned} \sum_{j=1}^8 T_j^e \left( \int_{\Omega^e} \frac{\partial \psi_j}{\partial x} \frac{\partial \psi_i}{\partial x} + \frac{\partial \psi_j}{\partial y} \frac{\partial \psi_i}{\partial y} + \frac{\partial \psi_j}{\partial z} \frac{\partial \psi_i}{\partial z} \, dx dy dz \right) \\ + \sum_{j=1}^4 T_j^e \left( \frac{c_{j,2}}{4c_1} \int_{\Gamma^e} \frac{\partial \psi_j}{\partial \mathbf{t}_{j,1}} \psi_i \, dx dy \right. \\ \left. + \frac{c_{j,3}}{4c_1} \int_{\Gamma^e} \frac{\partial \psi_j}{\partial \mathbf{t}_{j,2}} \psi_i \, dx dy \right) \\ = \sum_{j=1}^4 \int_{\Gamma^e} \frac{-\delta g_j}{4c_1} \psi_i \, dx dy + \sum_{j=1}^8 \int_{\partial \Omega^e \setminus \Gamma^e} q_n \psi_i \, dx dy, \end{aligned} \tag{15}$$

where index  $j = 1, \dots, 4$  refers to nodes of the element  $\Omega^e$  that lie on the bottom boundary  $\Gamma$  of the computational domain  $\Omega$ . As we can see in Eq. (15), in comparison with Macák et al. (2020), there are 8 tangent vectors corresponding to the nodes lying on the bottom boundary of the element belonging to  $\Gamma$ . The illustration can be seen in Fig. 2.

Now, we can write (14) and (15) in a compact matrix form

$$\mathbf{K}^e \mathbf{T}^e = \mathbf{Q}^e, \tag{16}$$

where  $\mathbf{K}^e = [K_{ij}]$  denotes an element stiffness matrix,  $\mathbf{T}^e = (T_1, \dots, T_8)$  is a column vector of unknowns and  $\mathbf{Q}^e$  denote the right-hand side vector.

To evaluate element matrices and vectors, we proceed the following way. We choose one basis function  $\psi_i$  per vertex  $N_i^e$ . Then, the function  $\psi_i$  is uniquely determined by choosing value 1 at  $N_i^e$  and 0 at every  $N_j^e, i \neq j$ , and we differentiate the basis functions with respect to a position of each node in Cartesian coordinates. For more details about basis functions, see, e.g. Reddy (2006) or Brenner and Scott (2002). To evaluate boundary integrals over a boundary  $\Gamma^e$

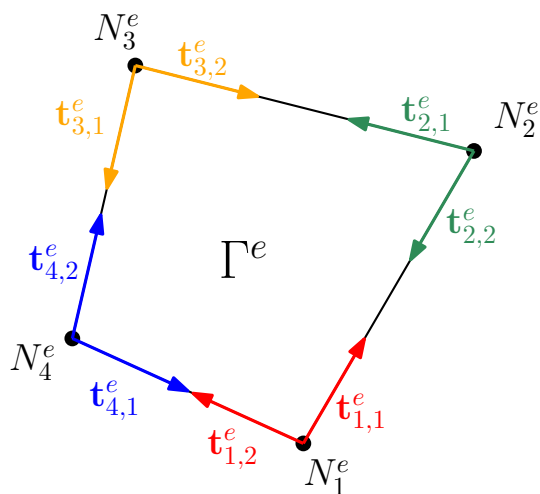


Fig. 2 Illustration of tangent vectors  $t_{i,j}^e$  to bottom boundary  $\Gamma^e$  at nodes  $N_i^e$  of an element  $\Omega^e$

in Eq. (15), which include tangential derivatives, we approximate derivatives in the tangential direction (see Fig. 2) like in the finite difference method. So using values of basis functions at nodes  $N_j^e$  of element  $\Omega^e$ , we have

$$\frac{\partial \psi_j}{\partial t_{j,1}} \approx \frac{\psi_j(N_{j+1}^e) - \psi_j(N_j^e)}{d(N_j^e, N_{j+1}^e)}, \tag{17}$$

$$\frac{\partial \psi_j}{\partial t_{j,2}} \approx \frac{\psi_j(N_{j-1}^e) - \psi_j(N_j^e)}{d(N_j^e, N_{j-1}^e)}, \tag{18}$$

where  $d$  denotes the distance between two neighbouring nodes that corresponds to the length of edge of an element  $\Omega^e$ .

### 3.4 Assembly of element equations

We assemble all element equations with using two principles:

- (i) continuity of primary variables at the interelement nodes. It means that nodal values  $T_j^e$  and  $T_j^{e+1}$  of two adjacent elements  $\Omega^e$  and  $\Omega^{e+1}$  at the connecting nodes have to be the same.
- (ii) “equilibrium” or “balance” equations of secondary variables at the interface between two elements. It means that on portions of  $\partial\Omega^e$  that are in the interior of the domain  $\Omega$ , the value  $q_n^e$  on the side  $p$  of the element  $\Omega^e$  cancels with the value  $q_n^{e+1}$  on the side  $r$  of the element  $\Omega^{e+1}$  when sides  $p$  of the element  $\Omega^e$  and  $r$  of the element  $\Omega^{e+1}$  are the same.

Finally, we take into account the Dirichlet BC (6) for nodes that lie on the  $\partial\Omega - \Gamma$ . In this way, we have obtained the

global linear system of equations with a column vector of unknown global nodal values  $\mathbf{T}$

$$\mathbf{KT} = \mathbf{Q}, \tag{19}$$

where the matrix  $\mathbf{K}$  is sparse, since most of its entries are zero and positive definite, and the column vector  $\mathbf{Q}$  whose entries are also almost zero except that for nodes with prescribed oblique derivative BC (5).

## 4 Numerical experiments

We present three different kinds of numerical experiments. At first, we investigate the so-called experimental order of convergence (EOC) of the derived FEM numerical scheme in several artificial testing experiments. Then, we try to reconstruct EGM2008 as a harmonic function over the extremely complicated Earth’s topography in the Himalayas and Tibetan Plateau. Finally, we apply the developed FEM approach to local gravity field modelling in Slovakia with the high-resolution  $100 \times 100$  m while using terrestrial gravity data.

### 4.1 Artificial testing experiments

As usual in numerical mathematics, at first we investigate the EOC of the FEM numerical scheme derived in Sect. 3. We perform several artificial experiments, the same as used for testing the EOC of the FEM scheme published in Macák et al. (2020). It aims to compare the EOC and stability of both FEM approaches. We start with reminding a definition of the EOC.

Let us assume that the error of the scheme in some norm is proportional to some power of the grid size, i.e.  $\|e_h\| = Ch^\alpha$ , with a constant  $C$ . The error of the scheme  $e_h$  is defined as a difference between the exact and numerical solution. Then, having two grids with the maximal diameter of the finite volumes  $h_{\max_1}$  and  $h_{\max_2}$ , where  $h_{\max_1} > h_{\max_2}$ , we can obtain numerically two errors  $\|e_{h_{\max_1}}\| = Ch_{\max_1}^\alpha$  and  $\|e_{h_{\max_2}}\| = Ch_{\max_2}^\alpha$ . We can see that

$$\frac{\|e_{h_{\max_1}}\|}{\|e_{h_{\max_2}}\|} = \frac{Ch_{\max_1}^\alpha}{Ch_{\max_2}^\alpha} = \left(\frac{h_{\max_1}}{h_{\max_2}}\right)^\alpha \tag{20}$$

from where we can extract

$$\alpha = \log_{\frac{h_{\max_1}}{h_{\max_2}}} \frac{\|e_{h_{\max_1}}\|}{\|e_{h_{\max_2}}\|}, \tag{21}$$

which is called the experimental order of convergence (EOC) of the scheme. We will use the numerical  $L_2$  norm for evaluating the EOC.

To test the EOC of the FEM numerical scheme derived in Sect. 3, we perform artificial experiments of the gravitational potential  $T(\mathbf{x})$  generated by a unit sphere with the center of gravity  $C$  for different grid sizes. The exact solution is given by  $T(\mathbf{x}) = \frac{1}{|\mathbf{x} - (x_C, y_C, z_C)|}$  and its values are used to generate the oblique derivative and the Dirichlet BC. To simulate the oblique vector in the oblique derivative BC, we have shifted the center of gravity  $C$  (see Fig. 3a) and, in addition, we have rotated this vector by an angle  $\pm\alpha$  (see Fig. 3b).

#### 4.1.1 Experiment 1: Shift of the center point

The computational domain has been a tesseroid bounded by two concentric spheres with radii  $r_1 = 1$  and  $r_2 = 2$ , and a coaxial cone with dimension  $(-\pi/4, \pi/4) \times (-\pi/4, \pi/4)$ . The oblique vector  $\mathbf{s}$  has been caused by a shift of the center  $C = [0.2, -0.3, -0.2]$  of the computational domain. Results are presented in Table 1.

It is evident that the numerical scheme, see Table 1, is stable and second-order accurate.

#### 4.1.2 Experiment 2: Shift of the center point and a rotation by an angle $\pm\alpha$

In the Experiment 2, the computational domain, the shift of the center point and BC have been the same as in Experiment 1, only we have added a rotation by an angle  $\pm\alpha = 60^\circ$ . Obtained results are presented in Table 2. Since this is a large value of an angle of rotation, for a comparison, we have also computed the same experiment using the method that was published in Macák et al. (2020). These results are presented Table 3.

One can observe, see Table 2, that the method presented in this paper is second-order accurate also in cases of rotation by such a large angle, while the method published in Macák et al. (2020) fails, see Table 3. It demonstrates the unstable behaviour of the old method in these extremal situations which vanishes if the method presented in this paper is employed.

## 4.2 Reconstruction of EGM2008 over the Himalayas

Next numerical experiments aim to demonstrate how precise we are able to reconstruct a harmonic function above the extremely complicated Earth's topography in the Himalayas and Tibetan Plateau. Namely, the EGM2008 geopotential model up to degree 2160 (Pavlis et al. 2012) has been used as a harmonic function. The upper boundary has been chosen at the altitude of 230 km above the reference ellipsoid corresponding to an average altitude of the GOCE satellite orbits. The bottom boundary has been given by grid points located on the Earth's surface. Their spacing in horizontal directions has been uniform. Their heights have been interpolated

from the SRTM30 PLUS topography model (Becker et al. 2009), see Fig. 4a. In these grid points, the first derivatives in the radial direction have been prescribed that represent the oblique derivative BC (Fig. 4b). On the rest of the boundary, the Dirichlet BC in form of the disturbing potential have been prescribed. All these BCs have been generated from the EGM2008 up to d/o 2160 using the GrafLab program (Bucha and Janák 2013).

Three experiments with different levels of the discretization were performed, namely the meshes with (i)  $501 \times 301 \times 25$ , (ii)  $1001 \times 601 \times 49$ , and (iii)  $2001 \times 1201 \times 97$  computational nodes. They approximately correspond to spacing  $0.1^\circ \times 0.1^\circ \times 10$  km,  $0.05^\circ \times 0.05^\circ \times 5$  km and  $0.025^\circ \times 0.025^\circ \times 2.5$  km. Remark: we have performed the same experiments as published in Medl'a et al. (2018) in order to compare efficiency of both approaches, i.e. FEM with FVM.

Figure 4c depicts the disturbing potential generated from EGM2008 on the Earth's surface as a known harmonic function that we have been reconstructing. Figure 4c–e presents residuals between the obtained FEM solutions and EGM2008 on the bottom boundary. The statistics of the corresponding residuals are summarized in Table 4. Similarly, statistics of residuals for all nodes in the whole 3D computational domain is in Table 5. Both tables clearly demonstrate that refinements of the discretization lead to higher accuracy of the FEM solution giving a better agreement with EGM2008. On the Earth's surface (Table 4), the standard deviations (SDs) of residuals are decreasing from 0.61 to 0.09  $\text{m}^2\text{s}^{-2}$  ( $\approx 7$  cm to 9 mm) and the maximal values from 7.19 to 0.76  $\text{m}^2\text{s}^{-2}$  ( $\approx$  from 7.3 dm to 7.7 cm). Such an improvement is achieved despite the fact that refinements of the discretization involve a more detailed consideration of the Earth's topography.

The obtained results also demonstrate that by a sufficient refining of the discretization we are able to reconstruct EGM2008 on such extremely complicated Earth's surface with the "cm-level" accuracy. To compare with the FVM approach, the maximal values are very similar; however, SDs in the FEM experiments are about 1.5 times better and the mean values almost 2 times smaller (compare Table 5 here with Table 3 in Medl'a et al. (2018)). This confirms a higher efficiency of the presented FEM approach.

## 4.3 Local gravity field modelling in Slovakia using terrestrial gravity data

### 4.3.1 Computational domain and input data

In the last numerical experiment, we apply the developed FEM approach to local gravity field modelling in Slovakia using terrestrial gravity data. The upper boundary has been again chosen at the altitude of 230 km above the reference ellipsoid (a mean altitude of the GOCE satellite orbits). Here, the Dirichlet BC has been prescribed in

**Fig. 3** Illustration of the 2D FEM grid on a sector of a circle. The oblique vector  $s$  depicted by red arises from (a) a shift of the center  $C$  of the computational domain, (b) a shift of the center  $C$  of the computational domain and a rotation by an angle  $\pm\alpha$ . The  $\pm\alpha$  means that on one element we modify the vector  $s_i^e$  by a value  $+\alpha$  and on its adjacent elements by  $-\alpha$

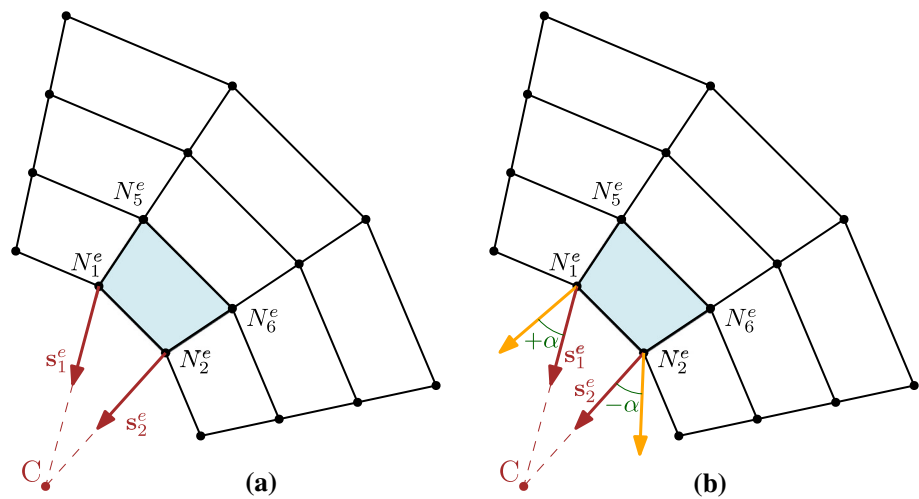


**Table 1** Experiment 1: Shift of the center point

No. of elements	$\ e_{h_{max}}\ _{L2}$	$EOC_{L2}$	$\ e_{h_{max}}\ _{MAX}$	$EOC_{MAX}$
$3 \times 3 \times 3$	$3.954 \times 10^{-2}$		$2.036 \times 10^{-1}$	
$6 \times 6 \times 6$	$4.043 \times 10^{-3}$	3.289	$1.730 \times 10^{-2}$	3.556
$12 \times 12 \times 12$	$7.627 \times 10^{-4}$	2.406	$3.512 \times 10^{-3}$	2.300
$24 \times 24 \times 24$	$1.683 \times 10^{-4}$	2.179	$8.005 \times 10^{-4}$	2.133
$48 \times 48 \times 48$	$3.970 \times 10^{-5}$	2.084	$1.913 \times 10^{-4}$	2.064
$96 \times 96 \times 96$	$9.646 \times 10^{-6}$	2.041	$4.683 \times 10^{-5}$	2.031

**Table 2** Experiment 2: Shift of the center point and a rotation by an angle  $\pm\alpha = 60^\circ$

No. of elements	$\ e_{h_{max}}\ _{L2}$	$EOC_{L2}$	$\ e_{h_{max}}\ _{MAX}$	$EOC_{MAX}$
$3 \times 3 \times 3$	$1.669 \times 10^{-2}$		$8.167 \times 10^{-2}$	
$6 \times 6 \times 6$	$2.327 \times 10^{-3}$	2.842	$1.247 \times 10^{-2}$	2.710
$12 \times 12 \times 12$	$4.129 \times 10^{-4}$	2.494	$2.326 \times 10^{-3}$	2.422
$24 \times 24 \times 24$	$8.860 \times 10^{-5}$	2.220	$4.821 \times 10^{-4}$	2.270
$48 \times 48 \times 48$	$2.057 \times 10^{-5}$	2.106	$1.134 \times 10^{-4}$	2.087
$96 \times 96 \times 96$	$4.960 \times 10^{-6}$	2.052	$2.748 \times 10^{-5}$	2.045

the form of disturbing potential (Fig. 5) generated from the GO\_CONS\_GCF\_2\_DIR\_R6 satellite-only geopotential model up to d/o 300 (Bruinsma et al. 2014). In this way, our FEM solution has been fixed on the upper boundary to the gravity field information detected by the satellite missions CHAMP, GRACE and GOCE.

On 4 side boundaries, the Dirichlet BC has been prescribed as well. However, here the disturbing potential has been generated from the EIGEN-6C4 geopotential model up to d/o 2160 (Förste et al. 2014). Due to the fact that the side boundaries have been chosen quite close to the borders of Slovakia, the prescribed disturbing potential could not be generated

**Table 3** Experiment 2: Shift of the center point and a rotation by an angle  $\pm\alpha = 60^\circ$ . Results obtained by the method published in Macák et al. (2020)

No. of elements	$\ e_{h_{max}}\ _{L2}$	$EOC_{L2}$	$\ e_{h_{max}}\ _{MAX}$	$EOC_{MAX}$
$3 \times 3 \times 3$	$8.490 \times 10^{-3}$		$4.391 \times 10^{-2}$	
$6 \times 6 \times 6$	$9.119 \times 10^{-3}$	-0.103	$5.863 \times 10^{-2}$	-0.417
$12 \times 12 \times 12$	$2.388 \times 10^{-3}$	1.933	$2.076 \times 10^{-2}$	1.497
$24 \times 24 \times 24$	$2.257 \times 10^{-3}$	0.081	$2.031 \times 10^{-2}$	0.031
$48 \times 48 \times 48$	$2.313 \times 10^{-3}$	-0.035	$2.067 \times 10^{-2}$	-0.025
$96 \times 96 \times 96$	$2.323 \times 10^{-3}$	-0.006	$2.081 \times 10^{-2}$	-0.009

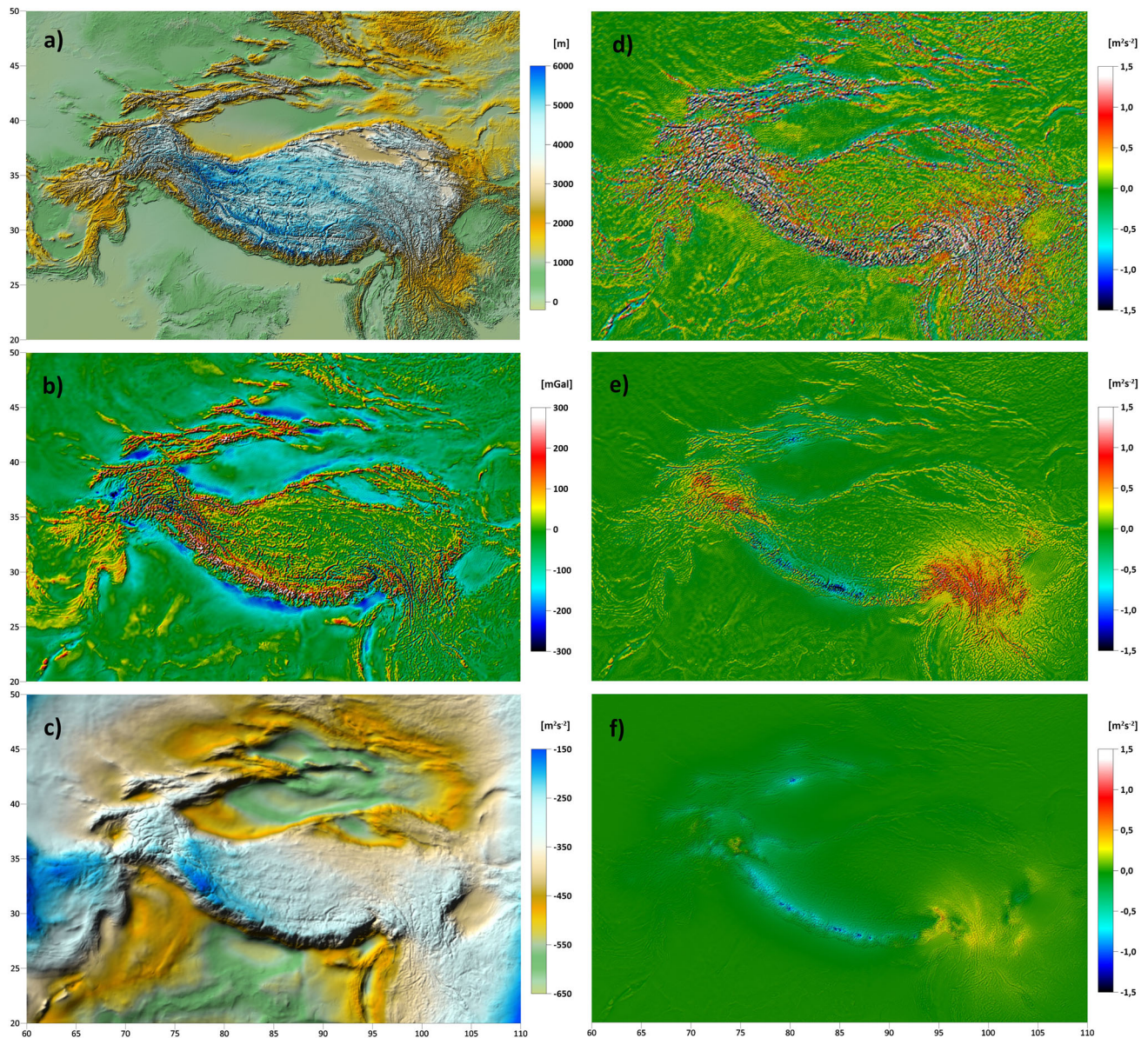


**Fig. 4** **a** The Earth's surface topography in the Himalayas and Tibetan Plateau (the bottom boundary), **b** gravity disturbances (the oblique derivative BC), **c** the disturbing potential generated from EGM2008 on the Earth's surface (a reconstructed harmonic function), and **d–f**

residuals between the FEM solutions and EGM2008 for different discretizations of the computational domain: **d**  $501 \times 301 \times 25$ ,  $1001 \times 601 \times 49$ , and **f**  $2001 \times 1201 \times 97$

**Table 4** Statistics of residuals between our FEM solution and EGM2008 on the bottom boundary in the Himalayas (units:  $\text{m}^2\text{s}^{-2}$ )

No. of nodes	$501 \times 301 \times 25$	$1001 \times 601 \times 49$	$2001 \times 1201 \times 97$
Min. value	-4.26	-5.69	-3.07
Mean value	0.17	0.01	-0.02
Max. value	7.19	2.12	0.76
St. deviation	0.61	0.17	0.09

**Table 5** Statistics of residuals between our FEM solution and EGM2008 in the whole 3D computational domain above the Himalayas (units:  $m^2s^{-2}$ )

No. of nodes	$501 \times 301 \times 25$	$1001 \times 601 \times 49$	$2001 \times 1201 \times 97$
Min. value	- 2.80	- 1.48	- 0.75
Mean value	0.95	0.41	0.18
Max. value	20.90	10.98	3.25
St. deviation	1.45	0.65	0.29

purely from satellite-only models. Otherwise, it would badly influence our numerical solution close to the side boundaries, especially near the Earth’s surface (Fašková et al. 2010).

In our numerical experiment, we have considered the Earth’s topography with the high horizontal resolution  $100 \times 100$  m (Fig. 6). At grid nodes on the bottom boundary,

the surface gravity disturbances as the oblique derivative BC have been prescribed (Fig. 7). Outside Slovakia, they have been interpolated from the GGMPlus database (Hirt et al. 2013). Inside Slovakia, the gravity disturbances have been generated from the detailed map of the complete Bouguer anomalies (Pašteka et al. 2017) using the CBA2G software

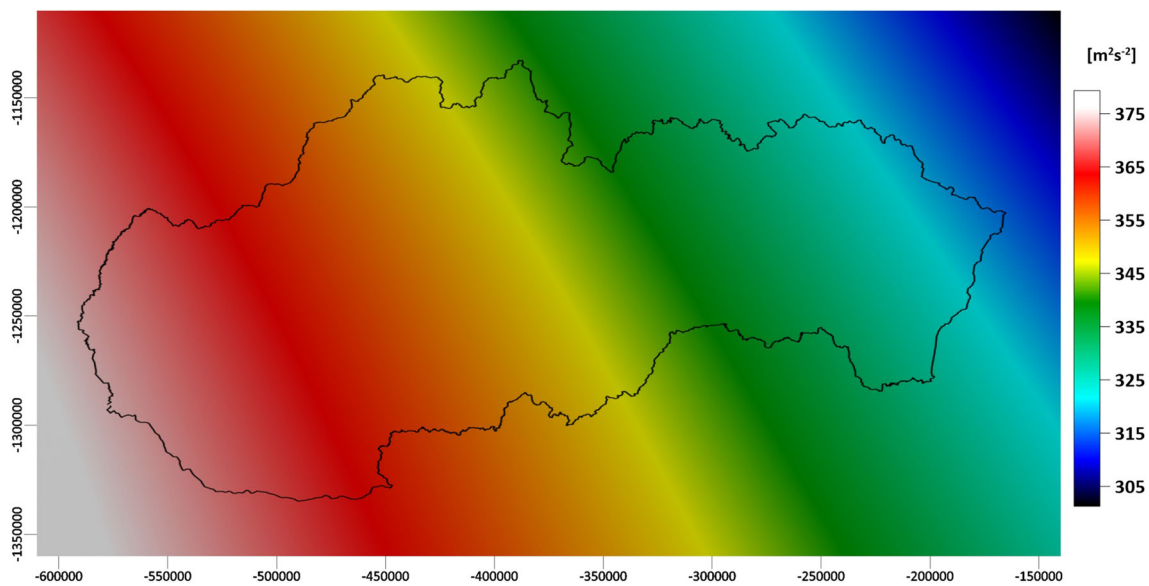


**Fig. 5** Disturbing potential at the altitude of 230 km above the reference ellipsoid as the Dirichlet BC on the upper boundary generated from the GO\_CONS\_GCF\_2\_DIR\_R6 model up to d/o 300

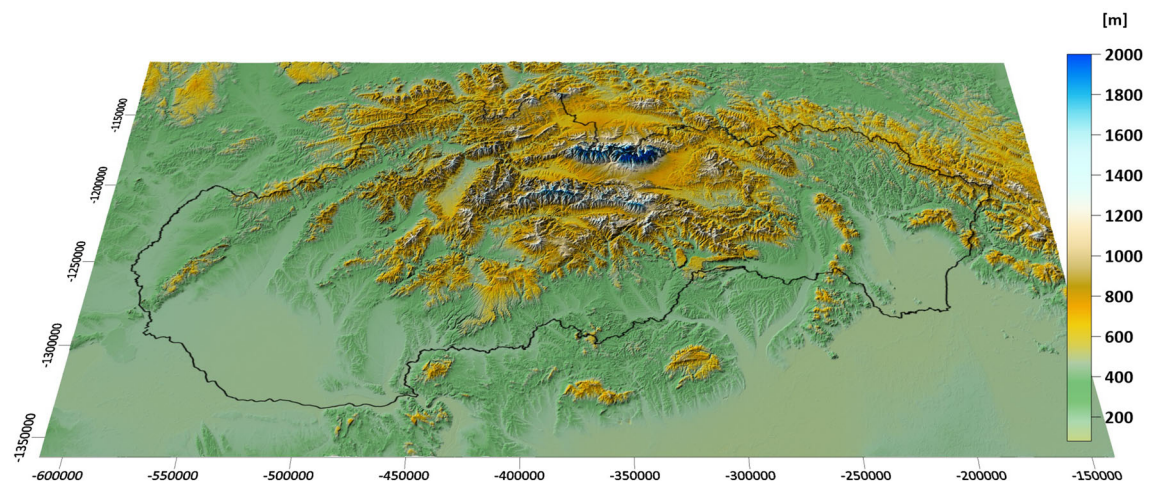


**Fig. 6** The Earth’s topography in area of Slovakia as a bottom boundary of the 3D computational domain (the horizontal resolution:  $100 \times 100$  m)

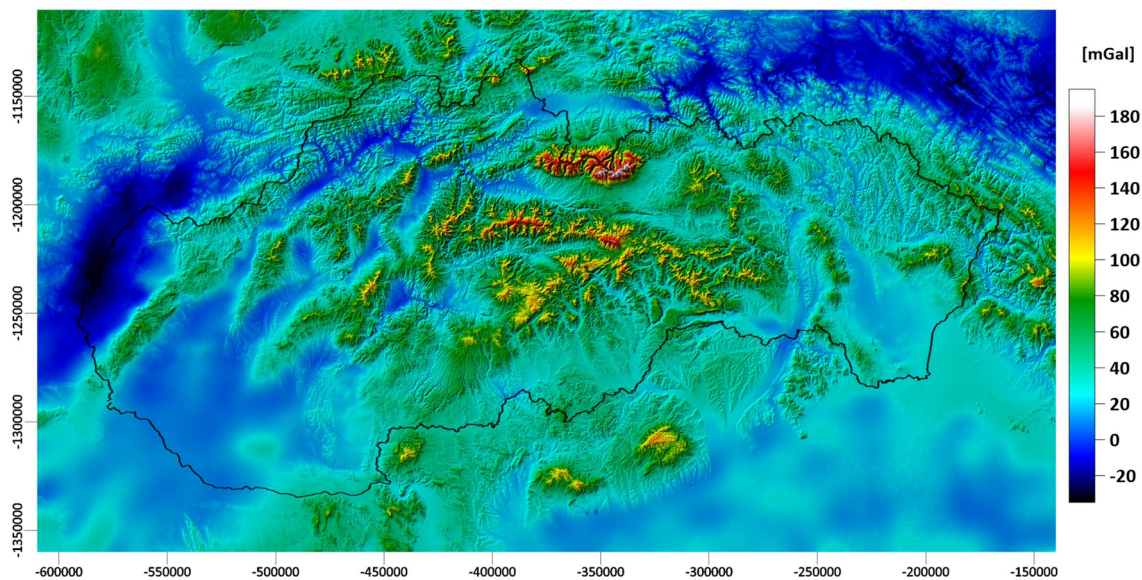


**Fig. 7** Gravity disturbances on the Earth's topography as the oblique derivative BC on the bottom boundary

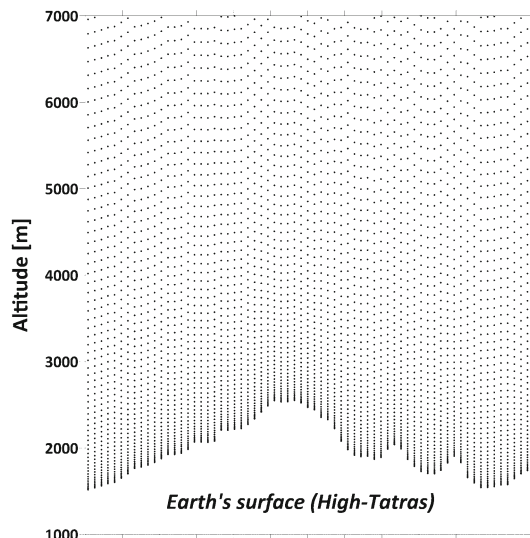


**Fig. 8** The sketch of lower computational nodes along the meridian profile crossing the High-Tatras (horizontal spacing: 100 m)

(Marušiak et al. 2015) and the detailed digital terrain model (see Acknowledgment). In this process, precise modelling of terrain corrections has played a crucial role, c.f. Majkráková et al. (2016) or Zahorec et al. (2017a). In this way, all information from the detailed terrestrial gravimetric mapping in Slovakia (Zahorec et al. 2017b) has been incorporated into the input data. All computations have been performed in the JTSK03 national coordinate system.

In the radial direction, the 3D computational domain has been discretized non-uniformly depending on altitude. According to our limits of memory access, we have divided the radial dimension into 450 parts. The radial size of finite

elements on the Earth's surface has been set to 10 m, while the radial size of finite elements above has been increasing linearly with increasing altitude exceeding 1 km for those on the upper boundary. Figure 8 depicts a sketch of lower computational nodes along the meridian profile crossing mountains of the High Tatras. To consider such non-uniform division is quite natural taking into account that the gravity field becomes smoother and smoother with increasing altitude.

#### 4.3.2 Computational aspects and derived quantities of the local gravity field

The computational domain has been discretized into the 3D unstructured mesh of finite elements which has consisted of  $4700 \times 2500 \times 450$  (longitude  $\times$  latitude  $\times$  height) = 5,287,500,000 elements in the whole computational domain (11,757,201 computational nodes on the discretized Earth's topography). A numerical solution of FGBVP using the developed FEM approach on such a large 3D unstructured mesh has required about 1.42 TB of internal memory. The final large-scale computations have been performed on 6 nodes of our cluster with 1.7 TB of distributed memory (each node consists of four 8-core CPUs with 256 GB RAM). Thanks to the NUMA (Non-Uniform Memory Access) architecture of each node, we have implemented a hybrid parallelization. Finally, the large-scale parallel computations were performed on 192 cores using 48 MPI processes, each with 4 OpenMP threads, taking about 90 h of the CPU time ( $\approx$  3.8 days). Such relatively high computational time was mainly caused by a slow convergence of the BiCGSTAB linear solver for such a detailed consideration of the Earth's

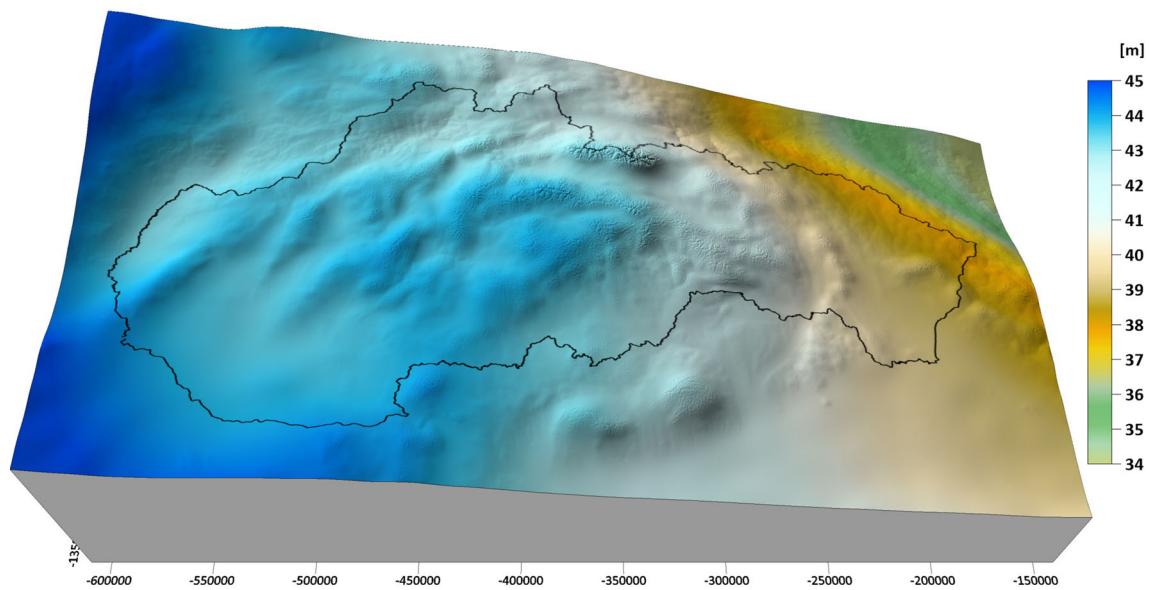


Fig. 9 Local quasigeoid model in Slovakia as the FEM numerical solution of FGBVP (the horizontal resolution: 100 m × 100 m)

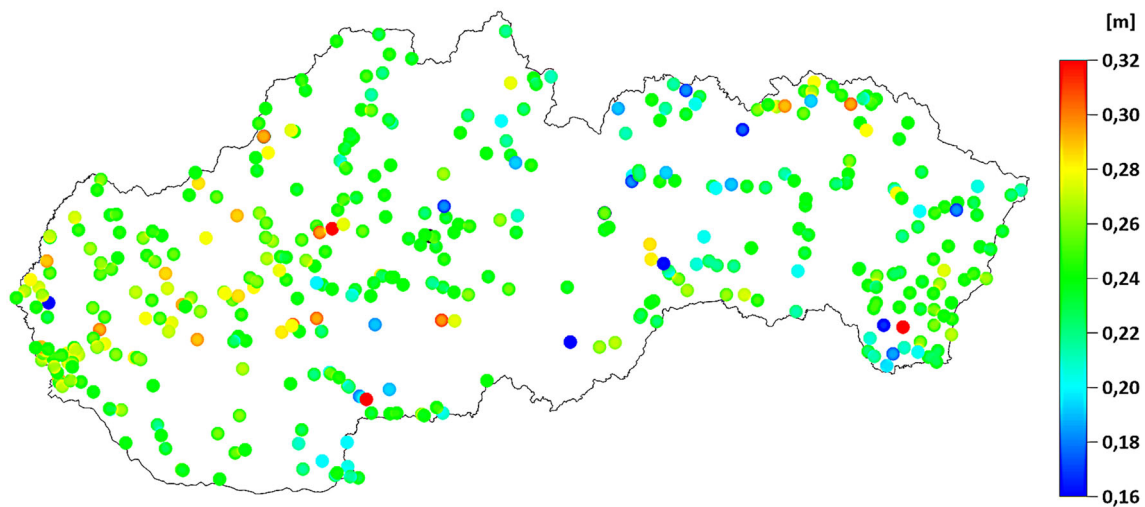


Fig. 10 GNSS/levelling test of the local quasigeoid model in Slovakia at 403 benchmarks

topography as well as due to the non-uniform discretization in the radial direction.

A benefit of such large-scale computations is that they have resulted in the disturbing potential obtained in every point of the whole 3D computational mesh, i.e. in all 5,287,500,000 elements. Hence, it is possible to derive different quantities of the local gravity field in every point, e.g. the first, second or higher derivatives in different directions. For example, we have evaluated the first and second derivatives in the radial direction in 5 altitude levels, i.e. approximately at 500 m, 1 km, 2 km, 5 km and 10 km above the reference ellipsoid. Figures in “Appendix” show how the gravity field is smoother and smoother with increasing altitude.

### 4.3.3 Local quasigeoid model in Slovakia and its GNSS/levelling test

To get a local quasigeoid model, the disturbing potential  $T$  obtained on the bottom boundary, i.e. at points directly on the Earth’s surface (Fig. 6), has been transformed into the quasigeoidal heights  $\xi$  using the formula

$$\xi_i = h_i - H_i^{\text{norm}} = h_i - \frac{-(T_i + U_i - W_0)}{\gamma_i} \tag{22}$$

where  $h$  is the ellipsoidal height,  $H^{\text{norm}}$  denotes the normal height,  $U$  is the normal potential evaluated at the  $i$ -th grid point on the Earth’s surface,  $\gamma$  is a mean value of the normal gravity between the quasigeoid and the Earth’s surface at this

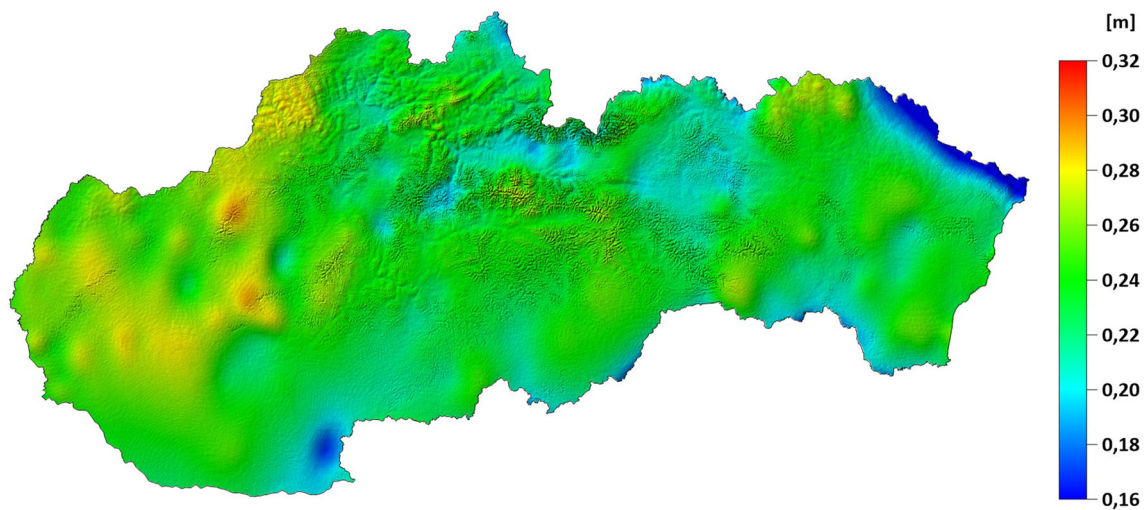


**Fig. 11** Differences between the obtained local quasigeoid model in Slovakia and DVRM05

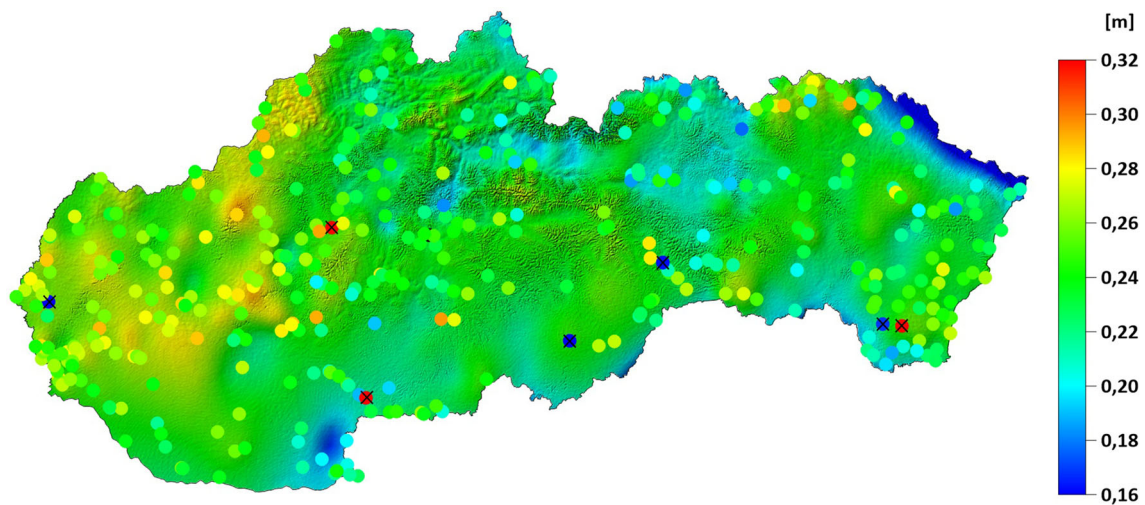


**Fig. 12** Overlapping the residuals at GNSS/levelling benchmarks with differences between the obtained local quasigeoid model and DVRM05 (7 identified outliers 'crossed')

**Table 6** Statistics of the GNSS/levelling test of the obtained local quasigeoid model in Slovakia

Characteristic	For all points	Without outliers
Points	403	396
Minimum	12.2 cm	15.6 cm
Maximum	34.9 cm	34.9 cm
Range	22.7 cm	19.3 cm
Mean	22.29 cm	22.31 cm
Median	22.28 cm	22.28 cm
STD	2.77 cm	2.54 cm

point, and  $W_0$  represents a reference value of the geopotential adopted for a realization of the International Height Reference System (IHRIS) (Sánchez et al. 2016). Parameters of

the normal gravity field have been computed from the WGS-84 reference ellipsoid. In this way, the quasigeoidal heights have been expressed with respect to the WGS-84 reference ellipsoid and to the  $W_0$  value adopted for IHRIS.

Figure 9 depicts the obtained local quasigeoid model in Slovakia with the resolution  $100 \text{ m} \times 100 \text{ m}$ . To validate its precision, the GNSS/levelling test has been performed at 403 benchmarks. Figure 10 depicts the obtained residuals. Their statistics is summarized in Table 6. The local quasigeoid model has been also compared with DVRM05 (Digital Vertical Reference Model), which is currently “an official model in Slovakia to transform ellipsoidal heights (determined by GNSS in the ETRS89 system) into sea level heights, namely into the normal heights in the Bpv vertical system” ([www.geoportal.sk](http://www.geoportal.sk)). This model was developed by polynomial fitting of a gravimetric-only quasigeoid to

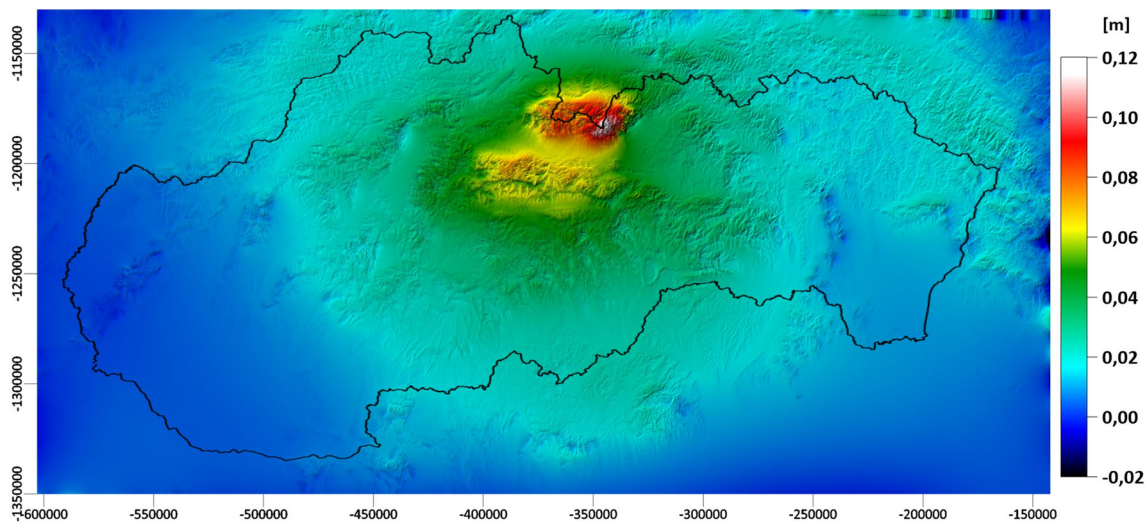


**Fig. 13** Differences between the local quasigeoid models in Slovakia obtained by FEM: the older numerical scheme (Macák et al. 2020) minus the presented new one

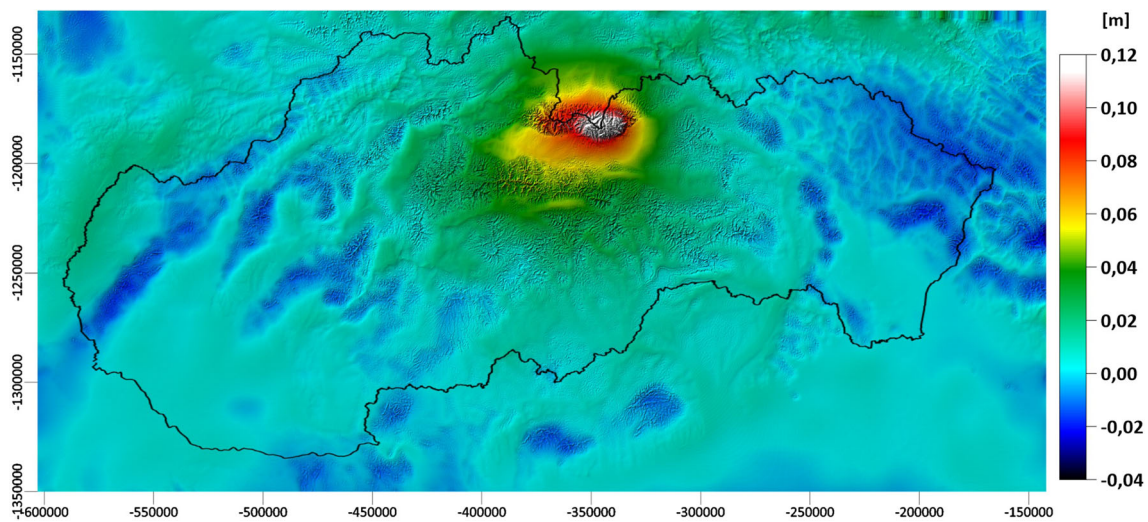


**Fig. 14** Differences between the local quasigeoid models in Slovakia: the FVM approach (Čunderlík et al. 2020) minus the presented FEM approach

304 GNSS/levelling benchmarks of the National Spatial Network of Slovakia (Klobušiak et al. 2005). Consequently, differences between both the models depicted in Fig. 11 show how the “GNSS-levelling quasigeoid” differs from our gravimetric-only quasigeoid. When overlapping both figures (Fig. 12), one can see a nice agreement except several points, where the colours are significantly different. These benchmarks have been identified as outliers (‘crossed’ in Fig. 12). Statistics of the GNSS/levelling test excluding these 7 outliers is presented in Table 6.

A mean value and median of the residuals of the GNSS/levelling test are 22.3 cm (Table 6). They indicate an offset of the national vertical datum of Slovakia with respect to  $W0 = 62,636\,853.4\text{ m}^2\text{s}^{-2}$  adopted as a reference value for a realization of IHR5 (Sánchez et al. 2016). SD of residuals is 2.77 cm and decreases to 2.54 cm after excluding 7

evident outliers (Table 6). It indicates high precision of the obtained local quasigeoid model.

#### 4.3.4 Comparison with recent local quasigeoid models in Slovakia

A comparison with the previous quasigeoid models in Slovakia shows that the obtained local quasigeoid model has outperformed all versions developed before 2016 while it is of a very similar quality as the recent ones. To see differences, we have compared our FEM solution with three different local quasigeoid models, namely with (i) one obtained by FEM using the older numerical scheme published in Macák et al. (2020) (Fig. 13), with (ii) one based on the FVM approach (Čunderlík et al. 2020) (Fig. 14), and with (iii) one computed in the spectral domain using a combination

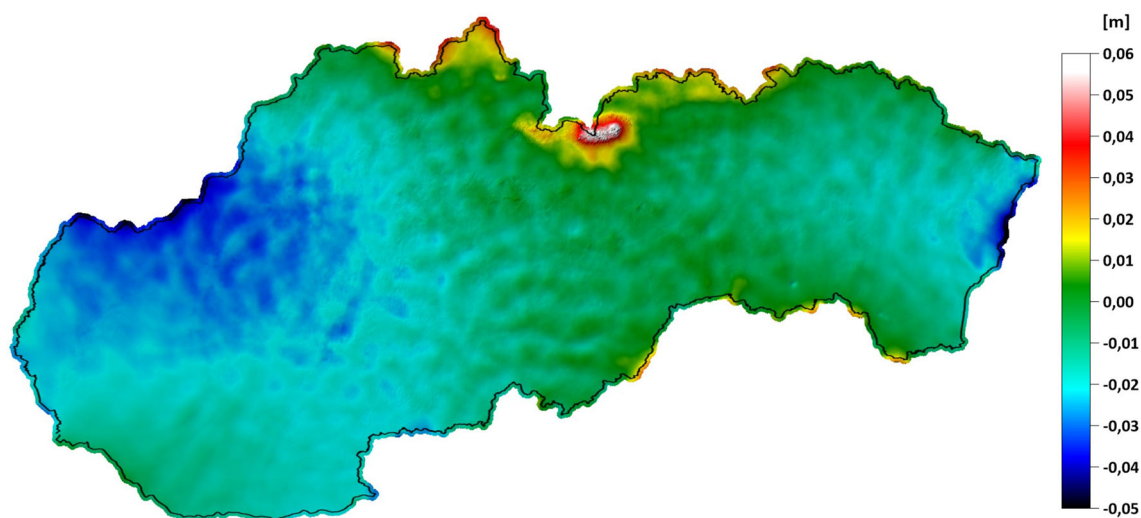


**Fig. 15** Differences between the local quasigeoid models in Slovakia: computed in the spectral domain (Bucha et al. 2016) minus the presented FEM approach

**Table 7** Statistics of the GNSS/levelling test of the recent quasigeoid models at 396 GNSS-levelling benchmarks

Local quasigeoid model	The new FEM approach cm	The previous FEM approach (Macák et al. 2020) cm	The FVM approach (Čunderlík et al. 2020) cm	Spherical Radial Basis Functions (Bucha et al. 2016) cm
Range	19.3	20.1	20.5	18.8
Mean	22.3	24.6	23.1	−53.7*
St. dev.	2.54	2.53	2.63	2.46

\*The mean value differs due to different transformation of the disturbing potential and related to the GRS-80 reference ellipsoid

of spherical harmonics, band-limited spherical radial basis functions and the residual terrain model technique (Bucha et al. 2016) (Fig. 15). In all cases, we have tested their precision at the same 396 GNSS/levelling benchmarks (excluding 7 aforementioned outliers). Table 7 depicts the statistics of GNSS/levelling test for all models.

SDs of residuals are very similar, and they differ less than 0.2 cm. The ranges of residuals are also very similar. Both quantities are slightly better for the model computed in the spectral domain (see Table 7), while the mean value is significantly different due to a different transformation of the disturbing potential (Bucha et al. 2016). Differences between the FEM or FVM numerical solutions depicted in Figures 13 and 14 show that the new FEM solution makes considerably lower undulation in areas of the highest mountains, especially in Tatra Mountains. The highest positive differences are in the High Tatras exceeding 10 cm. It means that here the quasigeoid undulation is more than 10 cm smaller. It is due to a different consideration of the oblique derivative BC where a stronger impact of the tangential components decreases the local undulation.

A comparison with the local quasigeoid model obtained in the spectral domain (Bucha et al. 2016) shows that the

differences have mainly a low-frequency character (Fig. 15). The negative differences up to -4 cm dominate in the western Slovakia and close to the border with Ukraine on the east. The positive differences are mainly close to the border with Poland on the north. The highest differences are again in the High Tatras where the quasigeoid undulation is more than 6 cm higher than in the FEM solution. Here, there is only one GNSS-levelling benchmark, in which the difference is +5.1 cm. Nevertheless, the low-frequency character of the differences and slightly better SD indicates a contribution of the low frequency part in the case of local gravity field modelling in the spectral domain.

Finally, we have also compared the FEM solutions when using the uniform and non-uniform discretization of the 3D computational mesh in the radial direction (see the sketch in Fig. 8). In the case of uniform spacing, the height of finite elements has been about 500 m. Figure 16 depicts how the non-uniform division contribute to the solution. It is evident that it makes higher undulation in the central part of Slovakia up to 4 cm. For the uniform division, the SD of residuals is 3.01 cm, which is 2.4 mm worse than in case of the non-uniform division.

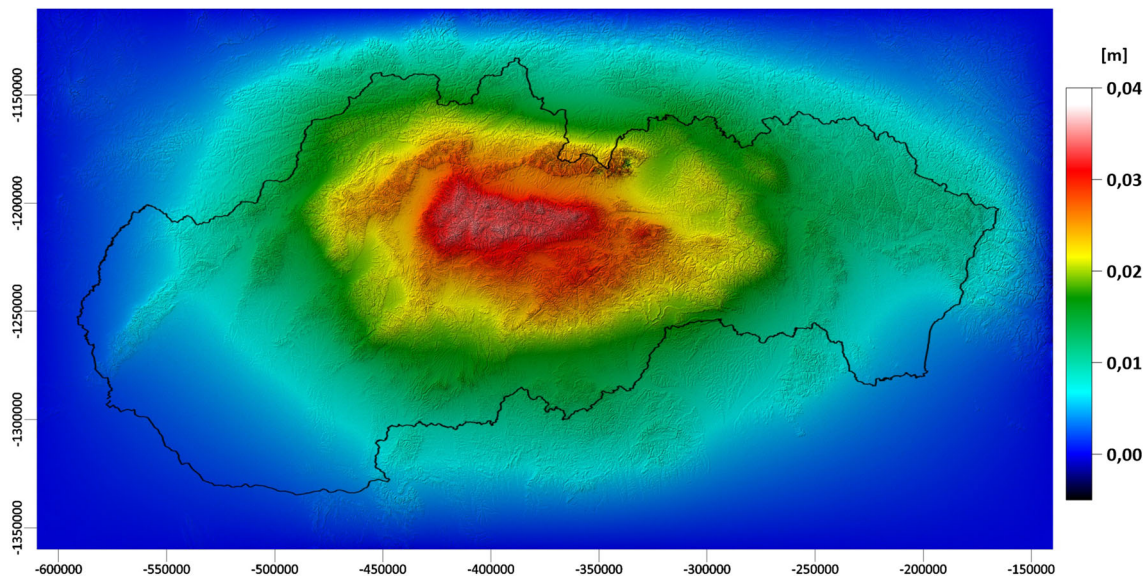


**Fig. 16** Comparison between the FEM solutions when using the uniform and non-uniform discretization of the 3D computational mesh in the radial direction

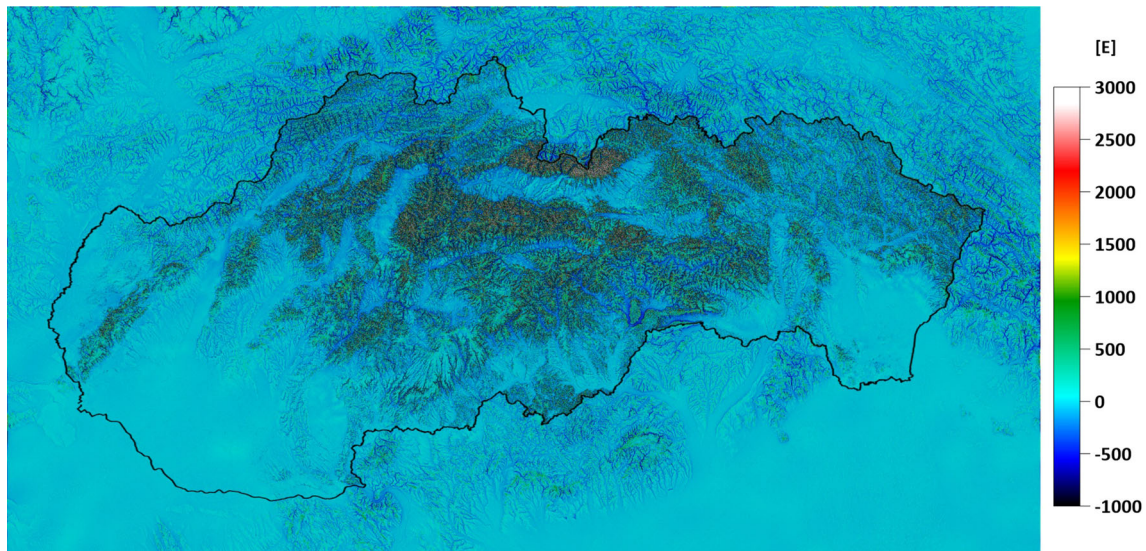


**Fig. 17** Gravity disturbing gradients  $T_{zz}$  evaluated numerically at grid points on the Earth's surface

#### 4.3.5 Surface gravity disturbing gradients and their testing

Our motivation to set the radial size of finite elements on the Earth's surface to 10 m and then use its linear increasing was (i) to capture better the local gravity field close to the Earth's surface, and (ii) to derive the second derivatives of the disturbing potential in the radial direction as precise as possible. Figure 17 depicts the gravity disturbing gradients  $T_{zz}$  evaluated numerically at grid points on the Earth's surface using finite differences. However, their testing by terrestrial measurements of the vertical gravity gradients (Zahorec et al. 2014) shows that our resolution  $100 \times 100$  m is still not sufficient to get satisfactory values. In areas of high mountains

or deep valleys, the Earth's topography is too smoothed for modelling such 'topography-sensitive' quantity. Moreover, available measurements of the gravity gradients were often performed in areas of the extremely complicated Earth's topography in order to observe extreme values, i.e. the highest or 'close-to-zero' vertical gradient of gravity (Zahorec et al. 2015). Nevertheless, after removing several points measured in extreme topography, the testing on 32 points shows the maximal difference 0.068 mGal/m, minimal difference  $-0.059$  mGal/m, mean value  $-0.008$  mGal/m and SD 0.029 mGal/m (290 E).

In the case of evaluating the second derivatives of the disturbing potential at different altitudes above the Earth's

surface (see Figures in “Appendix”), the horizontal resolution of the Earth’s topography  $100\text{ m} \times 100\text{ m}$  is sufficient. Here, the derived derivatives are not so topography-sensitive. Therefore, they better reflect the real gravity field and could be useful for geophysical investigations.

## 5 Conclusions and discussion

The presented FEM approach is solving the geodetic BVP with an oblique derivative BC numerically in a spatial domain. It allows to model gravity field directly on the discretized real Earth’s topography. The derived numerical scheme, in which the oblique derivative BC are considered directly in computational nodes located on the Earth’s surface, seems to be more efficient than our previous treatment based on their averaging over bottom sides of relevant finite elements (Macák et al. 2020). All numerical experiments have confirmed higher efficiency of the new numerical scheme, which avoids a loss of accuracy due to averaging. Artificial testing experiments have clarified that the presented FEM method is more stable and the second-order accurate.

Reconstruction of EGM2008 as a harmonic function over the Himalayas and Tibetan Plateau has shown that with a sufficient refinement of the discretization we are able to achieve “cm-level” accuracy, even on such extremely complicated Earth’s surface. A comparison with the results obtained by the FVM approach (Medl’á et al. 2018) has also confirmed a higher efficiency of the presented FEM approach.

The last numerical experiment has demonstrated that the developed FEM approach is suitable for very detailed and precise local gravity field modelling using terrestrial gravity data. The conceptual difference of our FEM approach treated ‘purely’ in the spatial domain in comparison with classical approaches based on the well-known ‘remove-compute-restore’ strategy is that we use low-frequency information detected from the satellite missions like CHAMP, GRACE or GOCE only on the upper and side boundaries. Here, our FEM solution is fixed to the GRACE/GOCE-based models by the Dirichlet BC; however, there is no information from the satellite missions in input data on the Earth’s surface as a bottom boundary.

This has obvious pros and cons. An advantage is that the impact of omission errors of the GRACE/GOCE-based satellite-only models on our FEM solution is considerably reduced, especially on the Earth’s surface. A drawback is that all systematic errors included in terrestrial gravimetric measurements as input data on the Earth’s surface, e.g. from an offset or tilt of vertical levelling networks, can fully influence obtained FEM solutions. In case of the spectral treatment, this drawback should be reduced.

A comparison of the FEM solution obtained in the spatial domain with the local quasigeoid model computed in the

spectral domain (Bucha et al. 2016) shows a low-frequency character of differences. The GNSS-levelling test confirms very similar accuracy of both models, while the standard deviations of residuals differ only by 0.1 mm. Taking into account accuracy of the GNSS-levelling benchmarks, we can state that the local gravity field modelling has reached such accuracy that it allows to detect some systematic tendencies in the vertical levelling network in Slovakia.

For local gravity field modelling in the spatial domain, a high density of terrestrial gravity data is extremely important in order to achieve sufficiently accurate result. Thus, the process of generating input gravity disturbances from the detailed map of the complete Bouguer anomalies (Pašteka et al. 2017) using the CBA2G software has played a crucial role in our experiment. However, an impact of the possible systematic tendencies hidden in input gravity disturbances should be investigated in this process.

Finally, we have to remind that detailed local gravity field modelling in the spatial domain using the presented FEM approach requires large-scale parallel computing. Obvious large memory requirements could seem as a limiting drawback. However, nowadays in era of HPC facilities such a drawback should not be a limiting, but rather challenging factor, which should motivate applications of the numerical methods like FEM, FVM or BEM for precise gravity field modelling. We believe that the results of presented numerical experiments have demonstrated that our FEM approach can reach the same quality as the state-of-the-art approaches nowadays used in physical geodesy.

**Acknowledgements** This work was supported by Grants APVV-15-0522, APVV-19-0460 and VEGA 1/0486/20. We would like express our thanks to Pavol Zahorec (SAV Banská Bystrica) and Juraj Papčo (STU Bratislava) for providing input gravity disturbances as well as measured vertical gravity gradients. We also thank the Geodetic and Cartographic Institute Bratislava for providing the GNSS/levelling data and to Blažej Bucha (STU Bratislava) for providing the local quasigeoid model in Slovakia published in Bucha et al. (2016).

**Author Contributions** Zuzana Minarechová contributed to develop the theory and wrote the manuscript with support from Róbert Čunderlík. Marek Macák developed the theory and performed the numerical simulations. Róbert Čunderlík carried out the experiment and analysed the data. Karol Mikula devised the project. All authors discussed the results and contributed to the final manuscript.

**Data availability** All datasets generated and/or analysed within the testing experiments (Sects 4.1 and 4.2) are available from the corresponding author. The input data used in Sect. 4.3 are not open for public as the authors do not have the rights to provide them to a third party. The output data of Sect. 4.3 are available from the corresponding author on reasonable request.

## Appendix

See Fig. 18.

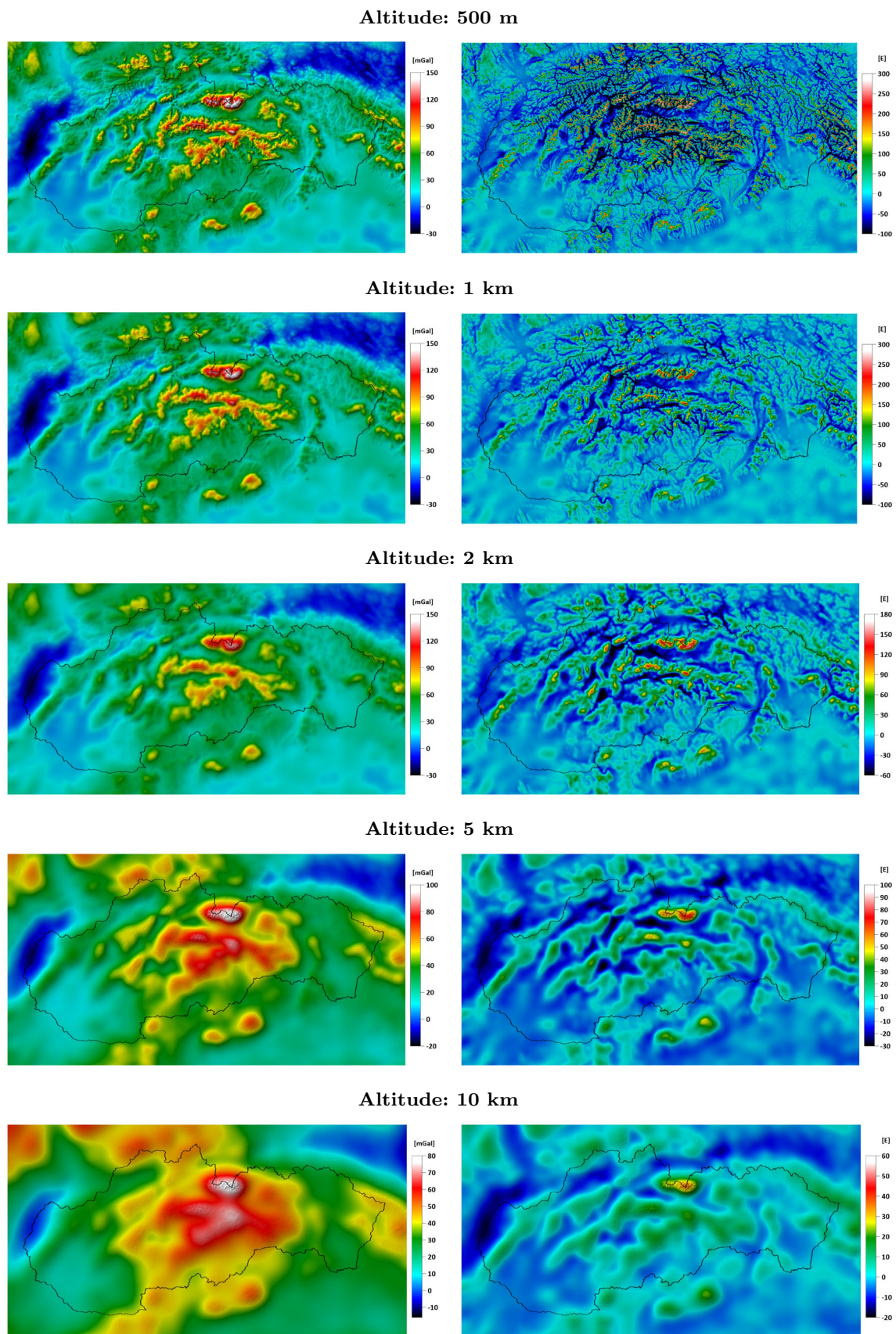


**Fig. 18** The first and second derivatives of the disturbing potential in the radial direction evaluated in 5 altitude levels (approximately at 500 m, 1 km, 2 km, 5 km and 10 km above the reference ellipsoid)

## References

- Barrett JW, Elliott CHM (1985) Fixed mesh finite element approximations to a free boundary problem for an elliptic equation with an oblique derivative boundary condition. *Comput Math Appl* 11(4):335–345
- Bauer F (2004) An alternative approach to the oblique derivative problem in potential theory. PhD thesis, Geomathematics Group, Department of Mathematics, University of Kaiserslautern. Shaker Verlag, Aachen, Germany
- Becker JJ, Sandwell DT, Smith WHF, Braud J, Binder B, Depner J, Fabre D, Factor J, Ingalls S, Kim SH, Ladner R, Marks K, Nelson S, Pharaoh A, Trimmer R, Von Rosenberg J, Wallace G, Weatherall P (2009) Global bathymetry and elevation data at 30 arc seconds resolution: SRTM30 PLUS. *Mar Geodesy* 32(4):355–371
- Bitzadse AV (1968) Boundary-value problems for second-order elliptic equations. North-Holland, Amsterdam
- Bjerhammar A, Svensson L (1983) On the geodetic boundary value problem for a fixed boundary surface. A satellite approach. *Bull Geod* 57(1–4):382–393
- Brenner SC, Scott LR (2002) The mathematical theory of finite element methods. Springer, New York
- Bruinsma S, Förste C, Abrikosov O, Lemoine J, Marty J, Mulet S, Rio M, Bonvalot S (2014) ESA's satellite-only gravity field model via the direct approach based on all GOCE data. *Geophys Res Lett* 41(21):7508–7514. <https://doi.org/10.1002/2014GL062045>
- Bucha B, Janák J (2013) A MATLAB-based graphical user interface program for computing functionals of the geopotential up to ultra-high degrees and orders. *Comput Geosci* 56:186–196. <https://doi.org/10.1016/j.cageo.2013.03.012>
- Bucha B, Janák J, Papčo J, Bezděk A (2016) High-resolution regional gravity field modelling in a mountainous area from terrestrial gravity data. *Geophys J Int* 207(2):949–966
- Čunderlík R, Mikula K (2010) Direct BEM for high-resolution gravity field modelling. *Stud Geophys Geod* 54(2):219–238
- Čunderlík R, Mikula K, Mojžeš M (2008) Numerical solution of the linearized fixed gravimetric boundary-value problem. *J Geod* 82:15–29
- Čunderlík R, Mikula K, Špir R (2012) An oblique derivative in the direct BEM formulation of the fixed gravimetric BVP. *IAG Sympos* 137:227–231
- Čunderlík R, Medl'a M, Mikula K (2020) Local quasigeoid modelling in Slovakia using the finite volume method on the discretized Earth's topography. *Contrib Geophys Geodesy* (accepted in June 2020)
- Droniou J, Medl'a M, Mikula K (2019) Design and analysis of finite volume methods for elliptic equations with oblique derivatives; application to Earth gravity field modeling. *J Comput Phys* 398:108876. <https://doi.org/10.1016/j.jcp.2019.108876>
- Fašková Z (2008) Numerical methods for solving geodetic boundary value problems. PhD Thesis, SvF STU, Bratislava, Slovakia
- Fašková Z, Čunderlík R, Janák J, Mikula K, Šprlák M (2007) Gravimetric quasigeoid in Slovakia by the finite element method. *Kybernetika* 43(6):789–796
- Fašková Z, Čunderlík R, Mikula K (2010) Finite element method for solving geodetic boundary value problems. *J Geod* 84(2):135–144
- Förste, Ch, Bruinsma, SL, Abrikosov O, Lemoine J-M, Marty JC, Flechtner F, Balmino G, Barthelmes F, Biancale R (2014) EIGEN-6C4 The latest combined global gravity field model including GOCE data up to degree and order 2190 of GFZ Potsdam and GRGS Toulouse. GFZ Data Services. <http://doi.org/10.5880/icgem.2015.1>
- Freeden W (1987) Harmonic splines for solving boundary value problems of potential theory. In: Mason JC, Cox MG (eds) *Algorithms for approximation*, vol 10. The Institute of Mathematics and its Applications, conference series. Clarendon Press, Oxford, pp 507–529
- Freeden W, Gerhards C (2013) Geomathematically oriented potential theory. CRC Press, Boca Raton
- Freeden W, Kersten H (1981) A constructive approximation theorem for the oblique derivative problem in potential theory. *Math Methods Appl Sci* 3:104–114
- Freeden W, Michel V (2004) Multiscale potential theory (with applications to geoscience). Birkhäuser, Boston
- Freeden W, Nutz H (2017) On the solution of the oblique derivative problem by constructive Runge–Walsh concepts. In: Pesenson I, Le Gia Q, Mayeli A, Mhaskar H, Zhou DX (eds) *recent applications of harmonic analysis to function spaces, differential equations, and data science*. Applied and numerical harmonic analysis. Birkhäuser, Cham
- Gallistl D (2019) Numerical approximation of planar oblique derivative problems in nondivergence form. *Math. Comp.* 88:1091–1119
- Gutting M (2007) Fast multipole methods for oblique derivative problems. PhD thesis, Geomathematics Group, Department of Mathematics, University of Kaiserslautern. Shaker Verlag, Aachen, Germany
- Gutting M (2012) Fast multipole accelerated solution of the oblique derivative boundary value problem. *Int J Geomath* 3:223–252
- Hirt C, Claessens SJ, Fecher T, Kuhn M, Pail R, Rexer M (2013) New ultra-high resolution picture of 1 Earth's gravity field. *Geophys Res Lett* 40
- Holota P (1997) Coerciveness of the linear gravimetric boundary-value problem and a geometrical interpretation. *J Geod* 71:640–651
- Kawecki E (2019) A discontinuous Galerkin finite element method for uniformly elliptic two dimensional oblique boundary-value problems. *SIAM J Numer Anal* 57(2):751–778
- Keller W (1995) Finite differences schemes for elliptic boundary value problems. Section IV Bulletin IAG, No, p 1
- Klees R (1995) Boundary value problems and approximation of integral equations by finite elements. *Manuscripta Geodaetica* 20:345–361
- Klees R, van Gelderen M, Lage C, Schwab C (2001) Fast numerical solution of the linearized Molodensky problem. *J Geodesy* 75:349–362
- Klobušiak M, Leitmannová K, Ferianc D (2005) Realizácia záväzných transformácií národných referenčných súradnicových a výškového Systému do Európskeho Terestrického Referenčného Systému 1989. <http://www.etr.sk/HELP/Transformacie> (in Slovak)
- Koch KR, Pope AJ (1972) Uniqueness and existence for the geodetic boundary value problem using the known surface of the earth. *Bull Geod* 46:467–476
- Lehmann R, Klees R (1999) Numerical solution of geodetic boundary value problems using a global reference field. *J Geodesy* 73:543–554
- Lieberman GM (2013) Oblique derivative problems for elliptic equations. World Scientific Publishing Co. Pte. Ltd., Hackensack
- Macák M, Minarechová Z, Mikula K (2014) A novel scheme for solving the oblique derivative boundary-value problem. *Stud Geophys Geo* 58(4):556–570
- Macák M, Čunderlík R, Mikula K, Minarechová Z (2015) An upwind-based scheme for solving the oblique derivative boundary-value problem related to the physical geodesy. *J Geodetic Sci* 5(1):15
- Macák M, Minarechová Z, Čunderlík R, Mikula K (2020) The finite element method as a tool to solve the oblique derivative boundary value problem in geodesy. *Tatra Mt Math Publ* 75(1):63–80
- Macák M, Mikula K, Minarechová Z (2012) Solving the oblique derivative boundary-value problem by the finite volume method. In: *ALGORITMY 2012*, 19th conference on scientific computing, Podbanske, Slovakia, September 9–14, 2012, Proceedings of contributed papers and posters, Publishing House of STU, pp 75–84
- Majkráková M, Papčo J, Zahorec P, Droščák B, Mikuška J, Marušiak I (2016) An analysis of methods for gravity determination and their

- utilization for the calculation of geopotential numbers in the Slovak national leveling network. *Contrib Geophys Geodesy* 46(3):179–202. <https://doi.org/10.1515/congeo-2016-0012>
- Marušiak I, Mikuška J, Papčo J, Zahorec P, Pašteka R (2015) CBA2G (Complete Bouguer Anomaly To Gravity), program for calculation of the gravity acceleration from complete Bouguer anomaly, program guide. Manuscript, G-trend Ltd
- Medl'a M, Mikula K, Čunderlík R, Macák M (2018) Numerical solution to the oblique derivative boundary value problem on non-uniform grids above the Earth topography. *J Geod* 92:1–19
- Meissl P (1981) The use of finite elements in physical geodesy. Report 313, Geodetic Science and Surveying, The Ohio State University
- Minarechová Z, Macák M, Čunderlík R, Mikula K (2015) High-resolution global gravity field modelling by the finite volume method. *Stud Geophys Geod* 59:1–20
- Miranda C (1970) Partial differential equations of elliptic type. Springer, Berlin
- Mráz D, Bořík M, Novotný J (2016) On the convergence of the h-p finite element method for solving boundary value problems in physical geodesy. In: Freymueller JT, Sánchez L (eds) International symposium on Earth and environmental sciences for future generations. International Association of Geodesy Symposia, vol 147. Springer, Cham
- Pašteka R, Zahorec P, Kušnirák D, Bošanský M, Papčo J, Szalaiová V, Krajňák M, Ivan M, Mikuška J, Bielik MM (2017) High resolution Slovak Bouguer gravity anomaly map and its enhanced derivative transformations: new possibilities for interpretation of anomalous gravity fields. *Contrib Geophys Geodesy* 47(2):81–94. <https://doi.org/10.1515/congeo-2017-0006>
- Pavlis NK, Holmes SA, Kenyon SC, Factor JK (2012) The development and evaluation of the Earth Gravitational Model 2008 (EGM2008). *J Geophys Res* 117:B04406. <https://doi.org/10.1029/2011JB008916>
- Reddy JN (2006) An introduction to the finite element method, 3rd edn. McGraw-Hill Education, New York
- Sánchez L, Čunderlík R, Dayoub N, Mikula K, Minarechová Z, Šíma Z, Vátr V, Vojtšková M (2016) A conventional value for the geoid reference potential  $W_0$ . *J Geodesy* 90(9):815–835. <https://doi.org/10.1007/s00190-016-0913-x>
- Shaofeng B, Dingbo C (1991) The finite element method for the geodetic boundary value problem. *Manuscr Geod* 16:353–359
- Šprlák M, Fašková Z, Mikula K (2011) On the application of the coupled finite-infinite element method to the geodetic boundary value problem. *Stud Geophys Geod* 55:479–487
- Zahorec P, Papčo J, Mikolaj M, Pašteka R, Szalaiová V (2014) The role of near topography and building effects in vertical gravity gradients approximation. *First Break* 32(1):65–71
- Zahorec P, Mikuška J, Papčo J, Marušiak I, Karcol R, Pašteka R (2015) Towards the measurement of zero vertical gradient of gravity on the Earth's surface. *Stud Geophys Geod* 59:524–537
- Zahorec P, Marušiak I, Mikuška J, Pašteka R, Papčo J (2017) Numerical calculation of terrain correction within the bouguer anomaly evaluation (Program Toposk), (Chapter 5). In: Pašteka R, Ján M, Bruno M (eds) Understanding the bouguer anomaly: a gravimetry puzzle. Elsevier, pp 79–92. ISBN 978-0-12-812913-5 <https://doi.org/10.1016/B978-0-12-812913-5.00004-X>
- Zahorec P, Pašteka R, Mikuška J, Szalaiová V, Papčo J, Kušnirák D, Pánisová J, Krajňák M, Vajda P, Bielik M, Marušiak I (2017) National gravimetric database of the Slovak Republic (chapter 7). In: Pašteka R, Ján M, Bruno M (eds) Understanding the bouguer anomaly: a gravimetry puzzle. Elsevier, pp 113–125. ISBN 978-0-12-812913-5,